Materials Research Letters

ISSN: (Print) 2166-3831 (Online) Journal homepage: https://www.tandfonline.com/loi/tmrl20

Enhanced void swelling in NiCoFeCrPd high-entropy alloy by indentation-induced dislocations

Chenyang Lu, Taini Yang, Ke Jin, Gihan Velisa, Pengyuan Xiu, Miao Song, Qing Peng, Fei Gao, Yanwen Zhang, Hongbin Bei, William J. Weber & Lumin Wang

To cite this article: Chenyang Lu, Taini Yang, Ke Jin, Gihan Velisa, Pengyuan Xiu, Miao Song, Qing Peng, Fei Gao, Yanwen Zhang, Hongbin Bei, William J. Weber & Lumin Wang (2018) Enhanced void swelling in NiCoFeCrPd high-entropy alloy by indentation-induced dislocations, Materials Research Letters, 6:10, 584-591, DOI: 10.1080/21663831.2018.1504136

To link to this article: https://doi.org/10.1080/21663831.2018.1504136

Published online: 08 Aug 2018.

MATER. RES. LETT.
2018, VOL. 6, NO. 10, 584–591
https://doi.org/10.1080/21663831.2018.1504136

MATERIALS RESEARCH LETTERS
Taylor & Francis
Taylor & Francis Group

ORIGINAL REPORT

Enhanced void swelling in NiCoFeCrPd high-entropy alloy by indentation-induced dislocations

Chenyang Lu [a], Taini Yang [a], Ke Jin [b], Gihan Velisa [b], Pengyuan Xiu [a], Miao Song [a], Qing Peng [a], Fei Gao [a], Yanwen Zhang [b], Hongbin Bei [b], William J. Weber [b,c] and Lumin Wang [a,d]

[a]Department of Nuclear Engineering and Radiological Sciences, University of Michigan, Ann Arbor, MI, USA; [b]Materials Science and Technology Division, Oak Ridge National Laboratory, Oak Ridge, TN, USA; [c]Department of Materials Science and Engineering, University of Tennessee, Knoxville, TN, USA; [d]Department of Materials Science and Engineering, University of Michigan, Ann Arbor, MI, USA

ABSTRACT

The role of dislocations on ion irradiation-induced void formation is studied in a high-entropy alloy (HEA) NiCoFeCrPd. Despite previous observations that show high-entropy alloys are swelling resistant due to a high defect recombination rate, the swelling is enhanced with increasing density of pre-existing dislocations at low strain levels that shortened transient duration before the onset of void swelling. Under certain irradiation conditions, a high density of dislocations may carry the material closer to the sink-dominated regime. Compared to another HEA NiCoFeCrMn, NiCoFeCrPd has a smaller loop size and higher loop density due to the stronger lattice distortion.

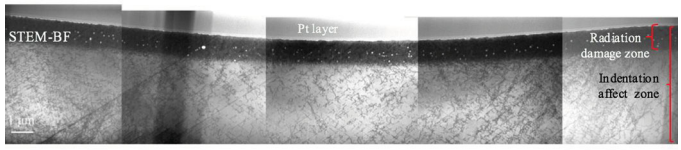

IMPACT STATEMENT

Swelling behavior in a newly designed high-entropy alloy NiCoFeCrPd has been studied for the first time. Void swelling is enhanced with increasing density of pre-existing dislocations in NiCoFeCrPd.

ARTICLE HISTORY
Received 23 February 2018

KEYWORDS
High-entropy alloy; ion irradiation; void swelling; dislocation loops

1. Introduction

Conventional alloys based on one or two principal elements and a small amount of alloying additions, such as steels, have been well designed and studied over the past centuries. In sharp contrast to conventional alloys, high-entropy alloys (HEAs), comprising of multiple principal elements all at high concentration or near equiatomic composition, have recently drawn great attention due to the potential for unique combinations of various properties derived from the huge unexplored compositional space of multicomponent alloys [1–6]. HEAs are defined by Yeh et al. [2] and named by Cantor et al. [1]. The name suggests that the entropy of mixing reaches its maximum for a stable solid solution phase. Excellent strength-ductility trade-off has been overcome in some HEAs at elevated, ambient and even cryogenic temperatures [3–5,7], which makes them candidate materials for many potential applications, e.g. advanced nuclear fission and fusion systems [3,7–9].

Equiatomic high-entropy alloy, NiCoFeCrMn, has been extensively investigated over a decade [1,3–5]. Five transition elements form a stable single-phase face-centered cubic (fcc) structure. This alloy displays excellent strength, ductility and toughness properties [3,4,10]. Furthermore, NiCoFeCrMn exhibits promising irradiation resistance as demonstrated by experimental studies [9,11–13]. A recent study reported a significant suppression of void swelling by two orders of magnitude in NiCoFeCrMn compared with that in pure nickel [12]. High-level distortion of electronic structure in

CONTACT Lumin Wang lmwang@umich.edu Department of Nuclear Engineering and Radiological Sciences, University of Michigan, Ann Arbor, MI 48109, USA; Department of Materials Science and Engineering, University of Michigan, Ann Arbor, MI 48109, USA; Chenyang Lu chenylu@umich.edu Department of Nuclear Engineering and Radiological Sciences, University of Michigan, Ann Arbor, MI 48109, USA

NiCoFeCrMn could change the process of energy dissipation and facilitate the recovery of radiation damage in the very early stages of irradiation [14,15]. Recently, a newly developed HEA, NiCoFeCrPd, shows comparable mechanical behaviors with NiCoFeCrMn, and even higher local distortion than NiCoFeCrMn, although knowledge of its irradiation response is very limited. In previous studies of concentrated solid solution alloys (CSAs), the effects of pre-existing defects (e.g. dislocations, precipitates, boundaries) on irradiation behavior have not been considered since the HEAs and other CSAs are mostly single-phase and well annealed with a very low density of dislocations and coarse grains for fundamental study. However, dislocation structures will eventually be introduced into the materials during the processing (cold rolling, shape forming, etc.) in practical applications. Therefore, a fundamental understanding on how the pre-existing dislocation structures affect the defect formation and accumulation is highly desired.

2. Materials and methods

The equiatomic NiCoFeCrPd alloy used in this study was prepared using the arc-melting method at Oak Ridge National Laboratory. The alloy has been confirmed to be a single-phase solid solution with an fcc structure [16]. The sample was chemical-mechanically polished to achieve a mirror-like surface with roughness below 3 nm. To study the role of dislocations on irradiation response, nanoindentation was intentionally conducted to deform the sample surface prior to ion irradiation, using a spherical sapphire indenter with a diameter of 200 μm. The nanoindentation was performed on a Nanoindenter XP at a constant $\dot{P}/P = 0.05\ s^{-1}$. The indentation depth of 2 μm was set for the sample, which resulted in residual depths of ~1.7 μm after the recovery of elastic displacement. The schematic of the spherical indentation test is shown in Figure 1(a). If we define *a* as the radius of the contact boundary, the depth of the idealized primary zone of indentation is about *2.4a* based on the Hertz's theory [17,18]. In our case, *a* is 15 μm, and thus the depth of idealized primary zone is about 36 μm. The indented sample was then irradiated by 3 MeV Ni^{2+} to a fluence of $5 \times 10^{16}/cm^2$ at 853 K in the Ion Beam Materials Laboratory at University of Tennessee [19]. In this set up, the deformed and un-deformed regions of the sample were irradiated simultaneously. A rastered beam was employed to ensure homogeneous irradiation. The schematic of irradiation on the indented region is shown in Figure 1(b). The depth of the radiation damage zone is about 1.5 μm calculated by Stopping Range of Ions in Matter (SRIM) 2013 code, which is equivalent to about *0.1a*. Based on the previous theoretical calculations, the strain introduced by spherical nanoindentation is relatively uniform from the sample surface to a depth of *0.1a* [18]. The peak damage level is ~50 dpa (displacement per atom) as calculated using SRIM in Kinchin-Pease mode with a displacement threshold energy of 40 eV.

Thin foils for transmission electron microscopy (TEM) studies were prepared using focused ion beam (FIB) equipped on an FEI Helios Nanolab dualbeam scanning electron microscopy (SEM). Transmission Kikuchi Diffraction (TKD) was also conducted on the Helios using an accelerating voltage of 20 keV with the

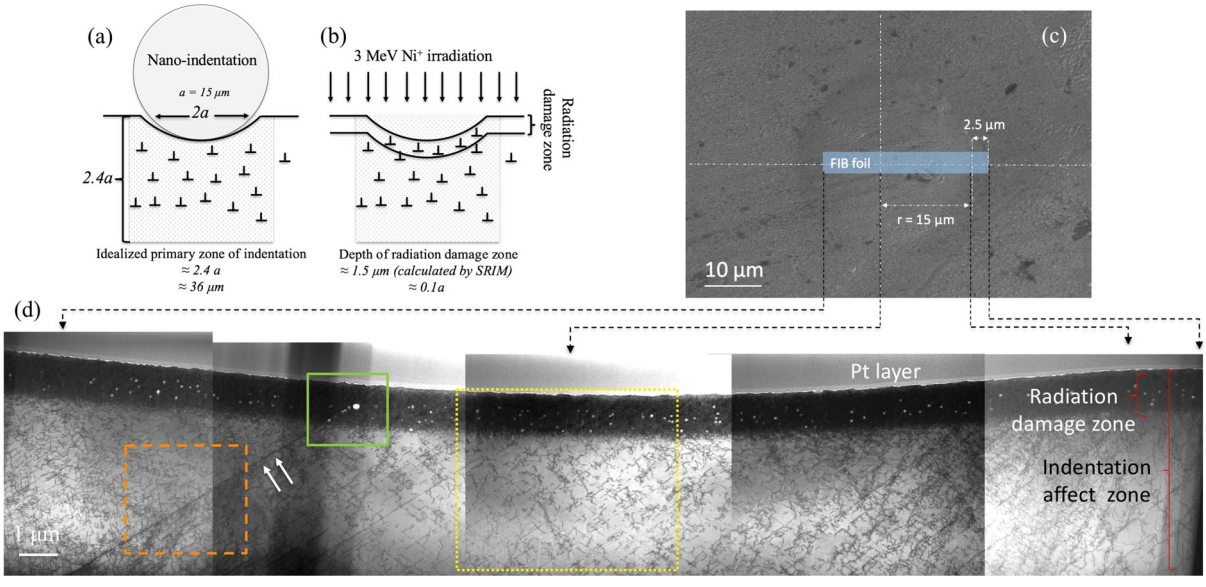

Figure 1. (a) Schematic of the indentation zone in spherical indentation; (b) schematic of the radiation damage zone in the indented sample; (c) SEM image of the spherical indentation; (d) cross-sectional STEM-BF image of indented sample.

TEM foil positioned at −20° relative to the incident electron beam. The step size for TKD scan was 15 nm. On-zone scanning TEM (STEM) with bright-field (BF) mode was employed for characterizing microstructures using a Cs-corrected JEOL 2100F. All irradiation- and deformation-induced features, including voids, dislocation loops and dislocation lines, can be imaged in a single micrograph because the multi-beam diffraction condition obtained by on-zone STEM-BF can maximize the visibility of most of the defect contents [5,6]. Furthermore, STEM-BF can image defect structures over a larger field than conventional TEM, while smearing out bend contour effects [20].

3. Results

Figure 1(c) shows the SEM image of the spherical indentation after 3 MeV Ni^{2+} irradiation. As shown in the image, the radius of the contact boundary is about 15 μm. A FIB foil was prepared right underneath the indentation for TEM characterization. The foil position is marked with a blue rectangle in Figure 1(c). Figure 1(d) shows the panoramic cross-sectional STEM-BF image of the foil prepared in Figure 1(c), where the material is highly stressed and strained. The related regions are linked by lines and arrows in Figure 1(c,d). The image was taken near the [110] zone axis. A dark band, manifesting the radiation damage zone, was observed from the sample surface to an extended depth. The darker contrast arose due to the high-density irradiation-induced dislocation loops. Imaging down the [110] zone axis in fcc alloy by STEM-BF can simultaneously capture faulted $<111>$ loops and perfect $<110>$ loops [20]. Voids, shown in white features, distributed relative uniformly in the radiation damage zone. While voids are the result of three-dimensional agglomeration of irradiation-induced vacancies, dislocation loops are often agglomerated by interstitials in fcc alloys [8]. Unlike the results obtained from un-indented single-phase concentrated alloys in previous studies [12], all survived interstitials and vacancies distributed in the cascade collision zone with no long-range separation along the depth in the indented NiCoFeCrPd alloy. This could be due to the possible trapping of defect clusters by deformation-induced structures .

Two grains are shown in Figure 1(d), with the grain boundary marked by white arrows. Beneath the radiation damage zone, a high density of dislocation structures introduced by indentation is observed. Clearly, dislocation slip occurred characteristically in several {111} planes. The dislocation gliding is one of the key deformation mechanisms under nanoindentation compression at room temperature. The observation on the dislocation formation is in good agreement with previous studies on fcc CSAs [5,6]. As shown in the orange rectangle with a dashed line in Figure 1(d), a higher density of dislocations was found near the grain boundary than in the interior of the grains, indicating that the dislocations were piled-up against the grain boundary wall. On the other hand, there is one huge void attached on the grain boundary which is much larger than the voids distributed in the interior of the grains, as shown in the green rectangle with a solid line in Figure 1(d). This may be due to the coalescence of vacancies and voids along the boundaries by fast pipe diffusion.

To further study the local deformation introduced by indentation, TKD technique was performed on the FIB foil sample. Figure 2 shows the panorama TKD maps of the same TEM foil shown in Figure 1(d). Figure 2(a), resulting from the combination of the image quality map (IQ) and inverse pole figure map (IPF), indicates that two grains are co-existing in the FIB sample. It is worth noting that although the features cannot match perfectly between on-zone STEM-BF image with IQ and IPF combination map due to the large angle tilt in TKD, we still can compare the microstructural features (e.g. grain boundary and the center of indentation) in Figure 1(d) and Figure 2. Figure 2(b) is a Kernel Average Misorientation (third order) map obtained by TKD that captures the small misorientations due to the dislocations and grain boundary. The map reveals various degrees of local strain distribution in the sample. The black regions, close to the middle-left, on the Kernel Average Misorientation map correspond to unindexed or low-confidence index data points. It is worth noting that the top layer colored by red is a protective Pt layer deposited before FIB milling. Beneath the Pt layer, especially in the region of the radiation damage zone, the strain distribution is relatively uniform as shown in Figure 2(b). Higher strain was observed in both the central region of the indentation and also the region near the grain boundary. This result partially supports the observation in the STEM-BF images that these two deformed regions have a high density of dislocation structures. The void and dislocation structures in the center of indentation, marked by a yellow rectangle of the dotted line in Figure 1(d), have been systematically studied to compare with the features in un-indented samples.

Figure 3(a,b) shows the cross-sectional STEM-BF images of the un-indented and indented NiCoFeCrPd samples after irradiation, respectively. The un-indented FIB sample was prepared from a region at least 50 ∼ 100 μm away from any indentation marks. The images were all taken near the [110] zone axis. The notable layers with a depth of ∼1 μm beneath the Pt layers in the two images contain high-density dislocation loops introduced by ion

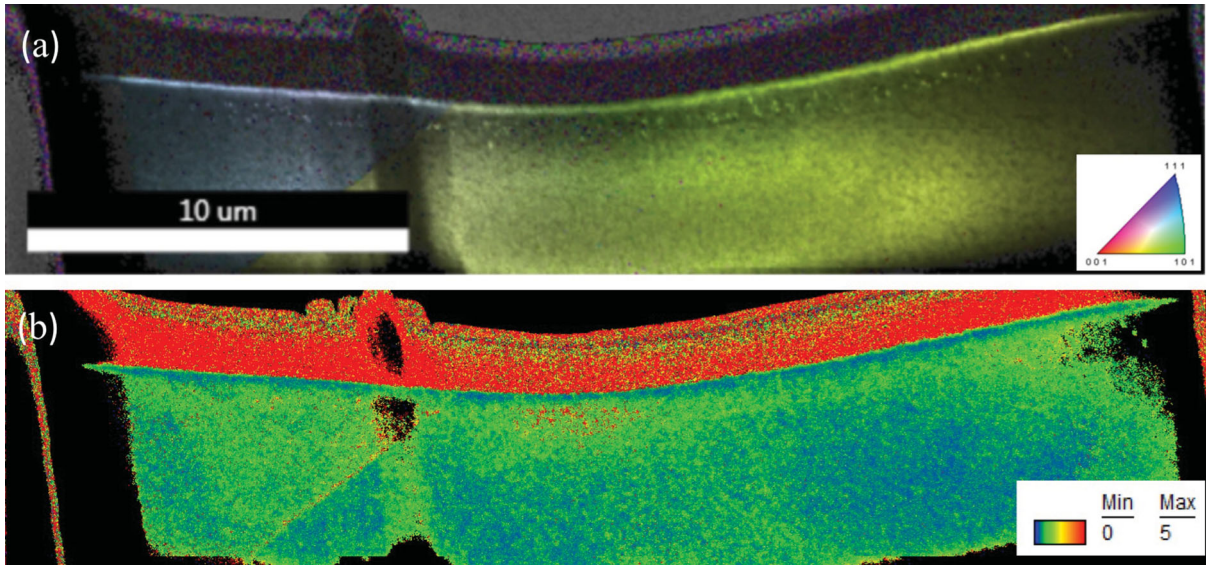

Figure 2. TKD results of indented NiCoFeCrPd after 3 MeV Ni^{2+} irradiation to a fluence of $5 \times 10^{16}/cm^2$ at 853 K. (a) Combination image of image quality map and inverse pole figure map; (b) Kernel average misorientation (third order) map.

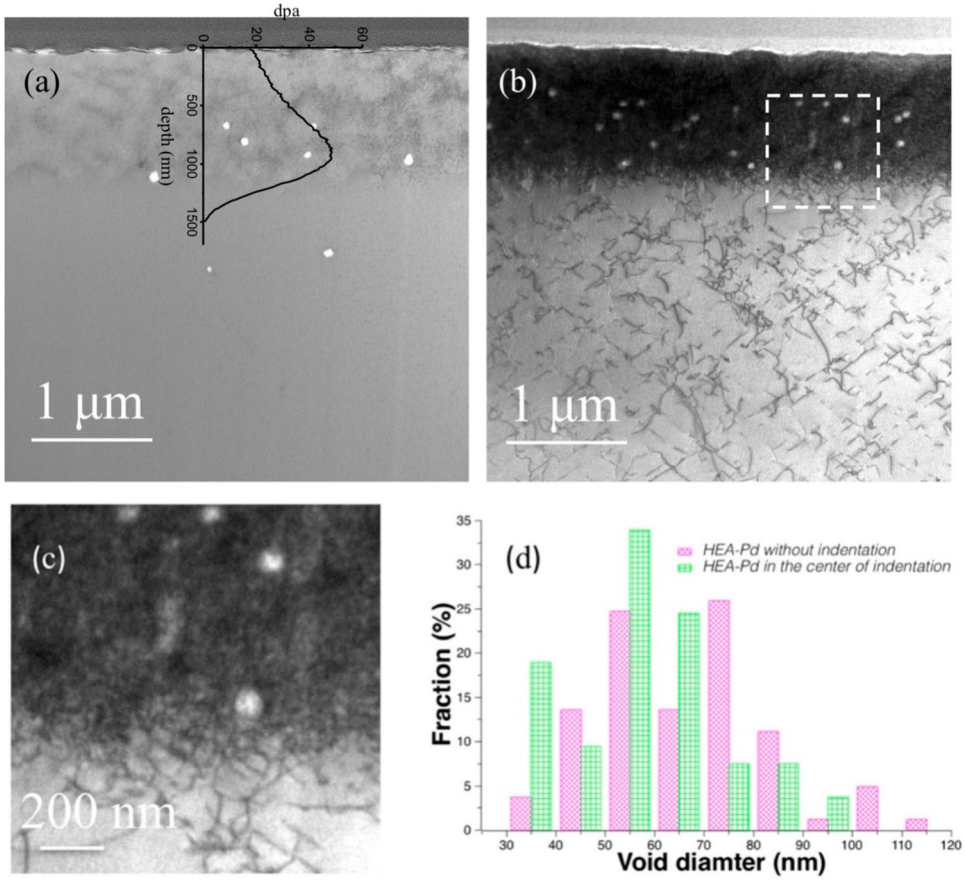

Figure 3. Cross-section STEM-BF images of (a) un-indented and (b) indented NiCoFeCrPd after irradiation to show the void and dislocation distributions; (c) Enlarged image from the area marked with a white dashed rectangle in (b) to show the high-density irradiation-induced dislocation loops and voids; (d) Void size distributions in un-indented and indented NiCoFeCrPd after irradiation.

irradiation. The enlarged image of dislocation loops is shown in Figure 3(c).

Note that a small density of dislocation lines, deeper than the irradiated layer (> 1.5 μm) shown in Figure 3(a),

Table 1. Statistics of microstructure features in ion-irradiated NiCoFeCrPd with or without pre-irradiation indentation.

	Dislocation density (10^{14}/m^2)	Void density (10^{20}/m^3)	Average void diameter (nm)	Swelling (%)	Loop density (10^{22}/m^3)	Average loop diameter (nm)
Un-indented NiCoFeCrPd	Very low	1.6 ± 0.12	67 ± 2.6	0.31 ± 0.08	3.5 ± 0.4	11.5 ± 1.2
Indented NiCoFeCrPd	0.59 ± 0.06	4.9 ± 0.25	62 ± 1.5	0.72 ± 0.1	6 ± 0.6	10.1 ± 1

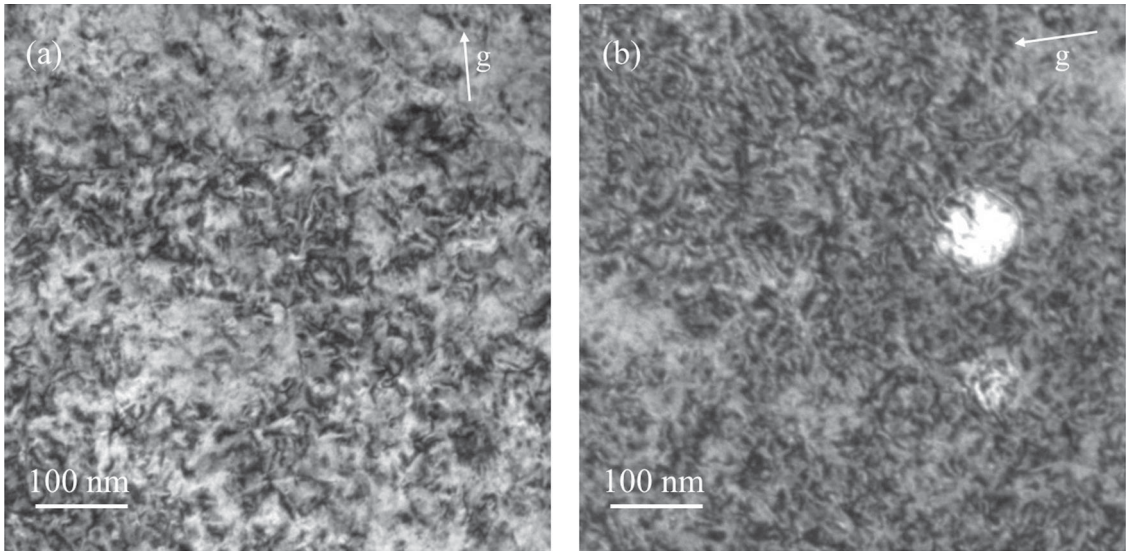

Figure 4. Dislocation loops in kinematic two-beam condition BF images of (a) un-indented and (b) indented NiCoFeCrPd after irradiation to a dose of 38 ± 5 dpa at 853 K. The two-beam condition $g = [200]$ is marked by the white arrow.

reveals that pre-existing dislocations are very low in the NiCoFeCrPd without irradiation or before indentation. After indentation, the density of dislocations increases significantly as shown in Figure 3(b). Ham's method was employed to quantitatively calculate the dislocation densities [5]. The result shows that the dislocation density in NiCoFeCrPd after indentation is about $0.59 \pm 0.06 \times 10^{14}$/m^2. This number is comparable to the previous study on the tensile tested NiCoFeCrMn at a true strain of 8.3% [5]. Furthermore, the microstructures of slip bands and dislocation pile-up are very similar in the indented NiCoFeCrPd and tensile tested NiCoFeCrMn at a true strain of 8.3% [5]. Therefore, although we don't know the accurate strain level in the indented NiCoFeCrPd, there is a comparable benchmark indicating that the indentation only introduced a relatively low strain level into the sample.

The void distributions are quite different in un-indented and indented sample regions as shown in Figure 3. For better accuracy, the statistics of voids were deduced from more than 5 TEM images with the foil thicknesses measured by Electron Energy Loss Spectroscopy (EELS). A comparison of void size distributions of the un-indented and indented sample regions is shown in Figure 3(d). The void distribution in the indented sample is shifted to slightly smaller sizes. The comparison of voids density, average void diameter and overall swelling is shown in Table 1. The results indicate that the average size of voids in the un-indented region (67 ± 2.6 nm) is slightly larger than in the indented region (62 ± 1.5 nm), but the density of the voids in the un-indented region ($1.6 \pm 0.12 \times 10^{21}$/m^3) is much smaller than in indented region ($4.9 \pm 0.25 \times 10^{21}$/m^3), leading to a higher overall swelling in the indented region ($0.72 \pm 0.1\%$) compared to that in the un-indented region ($0.31 \pm 0.08\%$). The results indicate that, under the irradiation condition in this work, a high-density of pre-existing dislocations lead to accelerated swelling, rather than enhanced defect annihilation.

Figure 4 shows the BF images of dislocations in un-indented and indented NiCoFeCrPd after irradiation. Two images in Figure 4 were taken under two-beam kinematical BF conditions using a diffraction vector $\mathbf{g} = 200$. The region of 600 ± 100 nm from the sample surface (38 ± 5 dpa) was chosen for the statistic of loop dislocation. The average loop size and density of the two samples are shown in Table 1. To be noted, the statistic of loop dislocation was deduced from more than 5 TEM images from each sample for accuracy. As shown in Table 1, indented NiCoFeCrPd has slightly smaller loops (10.1 ± 1 nm) than un-indented NiCoFeCrPd ($11.5.\pm 1.2$ nm), while the loop density in indented NiCoFeCrPd ($6 \pm 0.6 \times 10^{22}$/m^3) is higher than in un-indented NiCoFeCPd ($3.5 \pm 0.4 \times 10^{22}$/m^3). Although the loop nature is very

hard to identify due to the small size and extreme high density, however, it is believed that the dislocation loops are condensed by the interstitials based on the previous studies in SP-CSAs [12,15].

4. Discussion

High-entropy alloys are generically believed to be more radiation resistant due to a significantly enhanced recombination rate due to the high chemical complexity and lattice strain, and this has been demonstrated by several previous studies on samples free of pre-existing defects [12–15]. This study clearly indicated that when the dislocation density is high enough, the sink-dominated regime deprives interstitials for recombination can still be achieved in the high-entropy alloy to result in significant void nucleation and growth [21]. To achieve sink-dominated regime, three irradiation conditions are preferred, including sufficient dislocation density, high irradiation temperature and smooth dose rate. Firstly, in this study, the irradiation is temperature about $0.56T_m$ (melting temperature) of HEA-Pd, which is high enough to incline the system to a sink-dominated regime. Secondly, compared to the un-indented alloy, the dislocation density in the indented alloy (5.9×10^{13} m^{-2}) is several orders of magnitude higher, which provides sufficient density of sinks for interstitials. Thirdly, as long as the other irradiation conditions are met, high dose rate alone may not be able to prevent the material getting into or at least closer to the sink-dominated regime. Similar results have been reported by Leffers. In his study, the copper was irradiated using a high-voltage electron microscope with a high dose rate of 0.006–0.010 dpa/s. The void density and total swelling value were significant initially increased with the increased degree of cold work in pure copper [22]. It is worth noting that, the dose rate of neutron irradiations in advanced fission reactors and fusion reactors is several orders of magnitude lower than that for ion irradiation, which can further move the system to the sink-dominated regime. Based on that, we expect that in a real reactor system, the pre-existing dislocations may have a much higher possibility to enhance swelling during neutron irradiation in NiCoFeCrPd high-entropy alloy.

A low density of vacancies can also be introduced into the matrix by nanoindentation [23,24], however, their effects on void swelling can be ignored because the ion irradiation can introduce several orders of magnitude higher density of vacancies into the matrix (3.6×10^{20} vac/m^2) according to the SRIM calculation. Also, most of the indentation-induced vacancies may be annealed out during the heating process in irradiation experiments. It is generally considered that the pre-existing defects (e.g. dislocations, grain boundaries and precipitates) are the preferential stable sinks for vacancies and interstitials produced from cascade collisions, and dislocations are biased sinks for interstitials. Garner and his co-workers found that the cold working often accelerates the onset of void swelling in both bcc and fcc alloys [25–27], such as molybdenum and nickel. Leffers and his co-workers found a significant initial increase in void density and overall swelling value with the increased degree of cold work in pure copper [22]. At low cold work/strain levels, the introduced dislocations provide more nucleation sites for forming void embryos [22]. Void density and swelling value would level off, and eventually start decreasing with further cold work when vacancies can also reach the sinks easily. This explanation can be used to explain why the indented region of the sample in our study has a higher density of voids than the region with few dislocations. Furthermore, Garner and his co-workers claimed that, compared to cold worked alloys, void swelling is much more difficult to initiate in alloys with few dislocations, as the absence of network dislocations leads to a relatively long duration of the transient regime of void swelling before the onset of steady-state swelling. [25–27]. It is worth noting that voids distributed much deeper in the un-indented region of our sample than in the indented region as shown in Figure 3(a,b). In an un-indented sample, a certain number of vacancies have escaped from the radiation damage production zone to agglomerate into small voids in the deeper region. However, in the indented region, all voids were distributed in the radiation damage production zone, indicating that the pre-existing dislocations can efficiently prevent vacancy clusters from migrating to a deeper depth.

Comparing to other SP-CSAs alloys (NiFe, NiCoFe, NiCoFeCr, NiCoFeCrMn) [28], NiCoFeCrPd has a very small loop size and an extreme high loop density after irradiation. In author's previous study, four SP-CSAs alloys (NiFe, NiCoFe, NiCoFeCr, NiCoFeCrMn) were irradiated at 773 K to a same dose as in this study. NiCoFeCrMn has the smallest loop size (24 nm) and highest loop density ($1 \times 10^{22}/m^3$) among the four SP-CSAs alloy after irradiation [28]. It is generally considered that the loop size will increase and density will decrease with increasing irradiation temperature in fcc alloys, due to the loop growth and coalescence. In this study, NiCoFeCrPd was irradiated at a higher temperature (873 K). However, the loop size is still much smaller (11.5.±1.2 nm) and the density is much higher ($3.5 \pm 0.4 \times 10^{22}/m^3$) in NiCoFeCrPd irradiated at 853 K than in NiCoFeCrMn irradiated at 773 K. The result can be explained by the effect of local lattice distortion. According to the X-ray studies, NiCoFeCrPd has a stronger

local lattice distortion than NiCoFeCrMn, which effectively pins the irradiation-induced defects [29]. Therefore, NiCoFeCrPd can delay the loop evolution and growth compared to other SP-CSAs alloys. The higher local lattice distortion may come from the larger atomic volume deviation in NiCoFeCrPd compared to NiCoFeCrMn. The atomic volume size factors of Pd and Mn deviating from the atomic volume size of a nickel in the solid solutions are shown below. Much larger volume deviations from Ni are found in Pd (+41.33) than in Mn (+23.2%) [30]. Furthermore, nanoindentation can further introduce lattice distortion in NiCoFeCrPd and provide a high density of trap sites for the formation of interstitial-type dislocation loops. Therefore, indented NiCoFeCrPd has a smaller loop size and higher loop density than un-indented NiCoFeCrPd as shown in Table 1.

5. Conclusion

In summary, the irradiation response of a high-entropy alloy, NiCoFeCrPd, has been studied with and without high-density pre-existing dislocations. NiCoFeCrPd shows smaller loop size and higher loop density than NiCoFeCrMn and other SP-CSAs alloys because of the higher local lattice distortion. It is surprisingly found that, under certain irradiation conditions, void swelling may be enhanced with increasing dislocation density. Pre-existing dislocations can efficiently deprive interstitials for recombination and prevent vacancies from traveling a long distance, therefore making a significant impact on the void formation and distribution even in high-entropy alloys.

Disclosure statement

No potential conflict of interest was reported by the authors.

Funding

This work was supported as part of the Energy Dissipation to Defect Evolution (EDDE) Center, an Energy Frontier Research Center funded by the US Department of Energy, Office of Science, Basic Energy Sciences. Ion beam work was performed at the UT–ORNL Ion Beam Materials Laboratory located on the campus of the University of Tennessee–Knoxville. SEM and TEM characterizations were conducted in the Michigan Center for Material Characterization of the University of Michigan.

ORCID

Chenyang Lu http://orcid.org/0000-0002-3780-8420
Ke Jin http://orcid.org/0000-0001-7697-0466
Gihan Velisa http://orcid.org/0000-0003-4421-0790
Yanwen Zhang http://orcid.org/0000-0003-1833-3885
William J. Weber http://orcid.org/0000-0002-9017-7365

References

[1] Cantor B, Chang ITH, Knight P, et al. Microstructural development in equiatomic multicomponent alloys. Mater Sci Eng A. 2004;375–377:213–218.
[2] Yeh JW, Chen SK, Lin SJ, et al. Nanostructured high-entropy alloys with multiple principal elements: novel alloy design concepts and outcomes. Adv Eng Mater. 2004;6:299–303.
[3] Gludovatz B, Hohenwarter A, Catoor D, et al. A fracture-resistant high-entropy alloy for cryogenic applications. Science. 2014;345:1153–1158.
[4] Otto F, Yang Y, Bei H, et al. Relative effects of enthalpy and entropy on the phase stability of equiatomic high-entropy alloys. Acta Mater. 2013;61:2628–2638.
[5] Laplanche G, Kostka A, Horst OM, et al. Microstructure evolution and critical stress for twinning in the CrMnFeCoNi high-entropy alloy. Acta Mater. 2017;118:152–163.
[6] Laplanche G, Kostka A, Reinhart C, et al. Reasons for the superior mechanical properties of medium-entropy CrCoNi compared to high-entropy CrMnFeCoNi. Acta Mater. 2017;128:292–303.
[7] Wu Z, Bei H, Pharr GM, et al. Temperature dependence of the mechanical properties of equiatomic solid solution alloys with face-centered cubic crystal structures. Acta Mater. 2014;81:428–441.
[8] Zinkle SJ, Snead LL. Designing radiation resistance in materials for fusion energy. Annu Rev Mater Res. 2014;44:241–267.
[9] Zhang Y, Jin K, Xue H, et al. Influence of chemical disorder on energy dissipation and defect evolution in advanced alloys. J Mater Res. 2016;31:2363–2375.
[10] Gali A, George EP. Tensile properties of high- and medium-entropy alloys. Intermetallics. 2013;39:74–78.
[11] Zhang Y, Zhao S, Weber WJ, et al. Atomic-level heterogeneity and defect dynamics in concentrated solid-solution alloys. Curr Opin Solid State Mater Sci. 2017:1–17.
[12] Lu C, Niu L, Chen N, et al. Enhancing radiation tolerance by controlling defect mobility and migration pathways in multicomponent single-phase alloys. Nat Comms. 2016;7:1–8.
[13] Jin K, Lu C, Wang LM, et al. Effects of compositional complexity on the ion-irradiation induced swelling and hardening in Ni-containing equiatomic alloys. Scr Mater. 2016;119:65–70.
[14] Zhang Y, Stocks GM, Jin K, et al. Influence of chemical disorder on energy dissipation and defect evolution in concentrated solid solution alloys. Nat Comms. 2015;6:8736.
[15] Granberg F, Nordlund K, Ullah MW, et al. Mechanism of radiation damage reduction in equiatomic multicomponent single phase alloys. Phys Rev Lett. 2016;116:135504–135509.
[16] Jin K, Mu S, An K, et al. Thermophysical properties of Ni-containing single-phase concentrated solid solution alloys. Mater Des. 2017;117:185–192.
[17] Kalidindi SR, Pathak S. Determination of the effective zero-point and the extraction of spherical nanoindentation stress–strain curves. Acta Mater. 2008;56:3523–3532.
[18] Pathak S, Kalidindi SR. Spherical nanoindentation stress–strain curves. Mater Sci Eng R. 2015;91:1–36.

[19] Zhang Y, Crespillo ML, Xue H, et al. New ion beam materials laboratory for materials modification and irradiation effects research. Nucl Instit Methods Phys Res B. 2014;338:19–30.
[20] Parish CM, Field KG, Certain AG, et al. Application of STEM characterization for investigating radiation effects in BCC Fe-based alloys. J Mater Res. 2015;30:1–15.
[21] Sizmann R. Effect of radiation upon diffusion in metals. J Nucl Mater. 1978;69–70:386–412.
[22] Leffers T, Singh BN, Buckley SN, et al. Void-swelling in cold-worked copper during HVEM irradiation. J Nucl Mater. 1983;118:60–67.
[23] Hirth JP, Lothe J. Theory of dislocations. 2nd ed. Malabar: Krieger; 1992.
[24] Kiritani M, Sota T, Tawara T, et al. Defect structures introduced in FCC metals by high-speed deformation. Rad Eff Deffects Solids. 2002;157:53–74.
[25] Garner FA, Toloczko MB, Sencer BH. Comparison of swelling and irradiation creep behavior of fcc-austenitic and bcc-ferritic/martensitic alloys at high neutron exposure. J Nucl Mater. 2000;276:123–142.
[26] Dvoriashin AM, Porollo SI, Konobeev YV, et al. Influence of cold work to increase swelling of pure iron irradiated in the BR-10 reactor to ∼ 6 and ∼ 25 dpa at ∼ 400° C. J Nucl Mater. 2000;283:157–160.
[27] Konobeev YV, Dvoriashin A M, Porollo SI, et al. Swelling and microstructure of pure Fe and Fe–Cr alloys after neutron irradiation to ∼26dpa at 400°C. J Nucl Mater. 2006;355:124–130.
[28] Lu C, Jin K, Gao N, et al. Radiation-induced segregation on defect clusters in single-phase concentrated solid-solution alloys. Acta Mater. 2017;127:98–107.
[29] Tong Y, Velisa G, Zhao S, et al. Evolution of local lattice distortion under irradiation in medium- and high-entropy alloys. Materialia 2018; in press.
[30] King HW. Quantitative size-factors for metallic solid solutions. J. Mater. Sci. 1966;1:79–90.